Large-scale flow of Indian Ocean asthenosphere driven by Réunion plume

G. Barruol*[1,2], K. Sigloch[3], J.-R. Scholz[1,2], A. Mazzullo[1], E. Stutzmann[1], J.-P. Montagner[1], S. Kiselev[4], F. R. Fontaine[1,2], L. Michon[1,2], C. Deplus[1], J. Dyment[1]

1. Université de Paris, Institut de physique du globe de Paris, CNRS, UMR 7154, F-75005 Paris, France

2. Université de La Réunion, Laboratoire GéoSciences Réunion, F-97744 Saint Denis, France

3. University of Oxford, Earth Sciences Department, South Parks Road, Oxford OX1 3AN, UK.

4. Institute of Physics of the Earth, Moscow, Russia

SUPPLEMENTARY INFORMATION (SI)

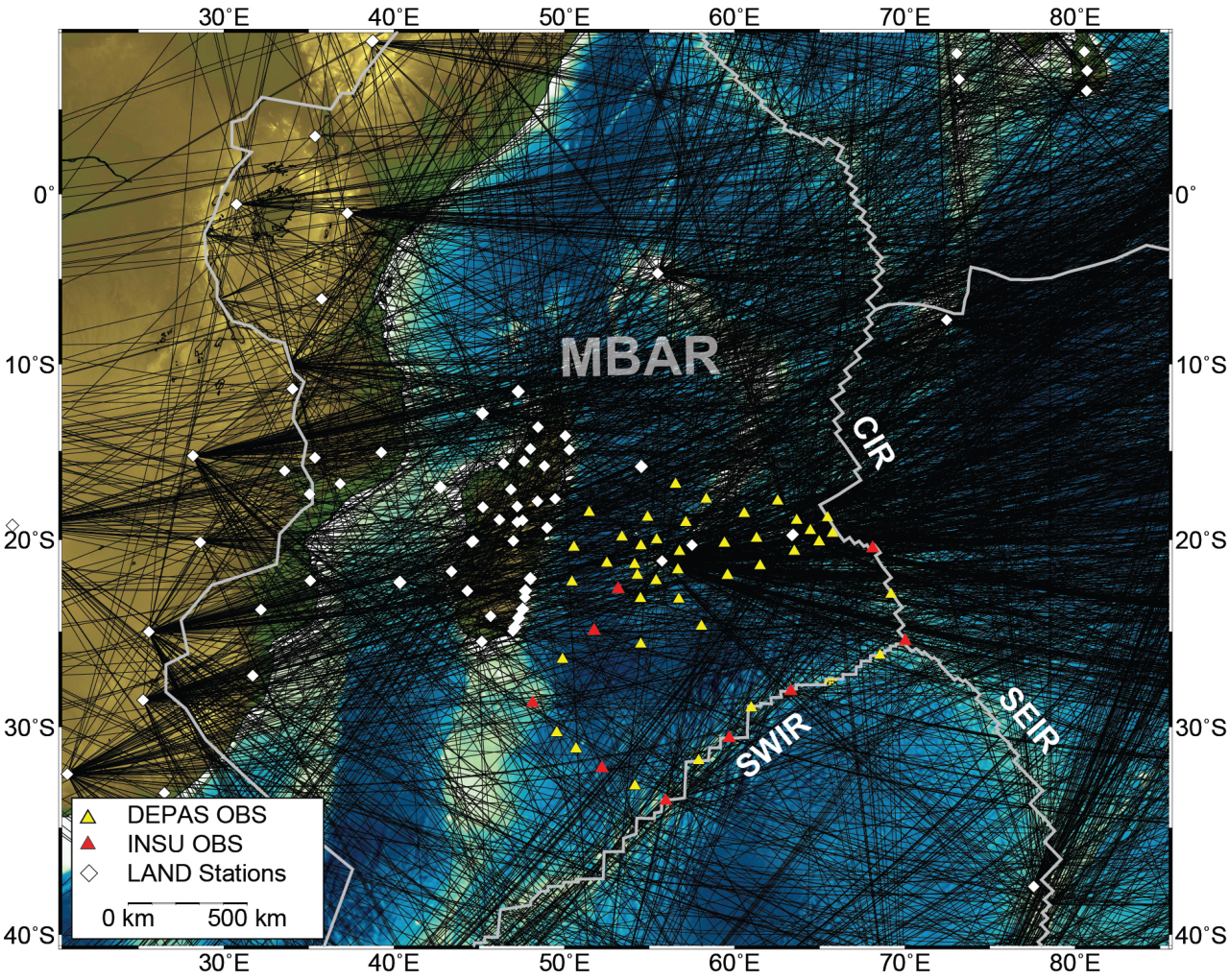

Figure S1

Figure S1: Map of the South-West Indian Ocean showing the RHUM-RUM network, including the German DEPAS OBS (yellow triangles) and the French INSU OBS (red triangles) stations deployed around Réunion, along the Central Indian Ridge (CIR) and the South-West Indian Ridge (SWIR). Also shown are the terrestrial seismic stations used (white diamonds), and the corresponding ray coverage used in the RHUM-RUM surface wave tomography[1]. "MBAR" indicates the centre of the Mascarene Basin Asthenosphere Reservoir discussed in the paper.

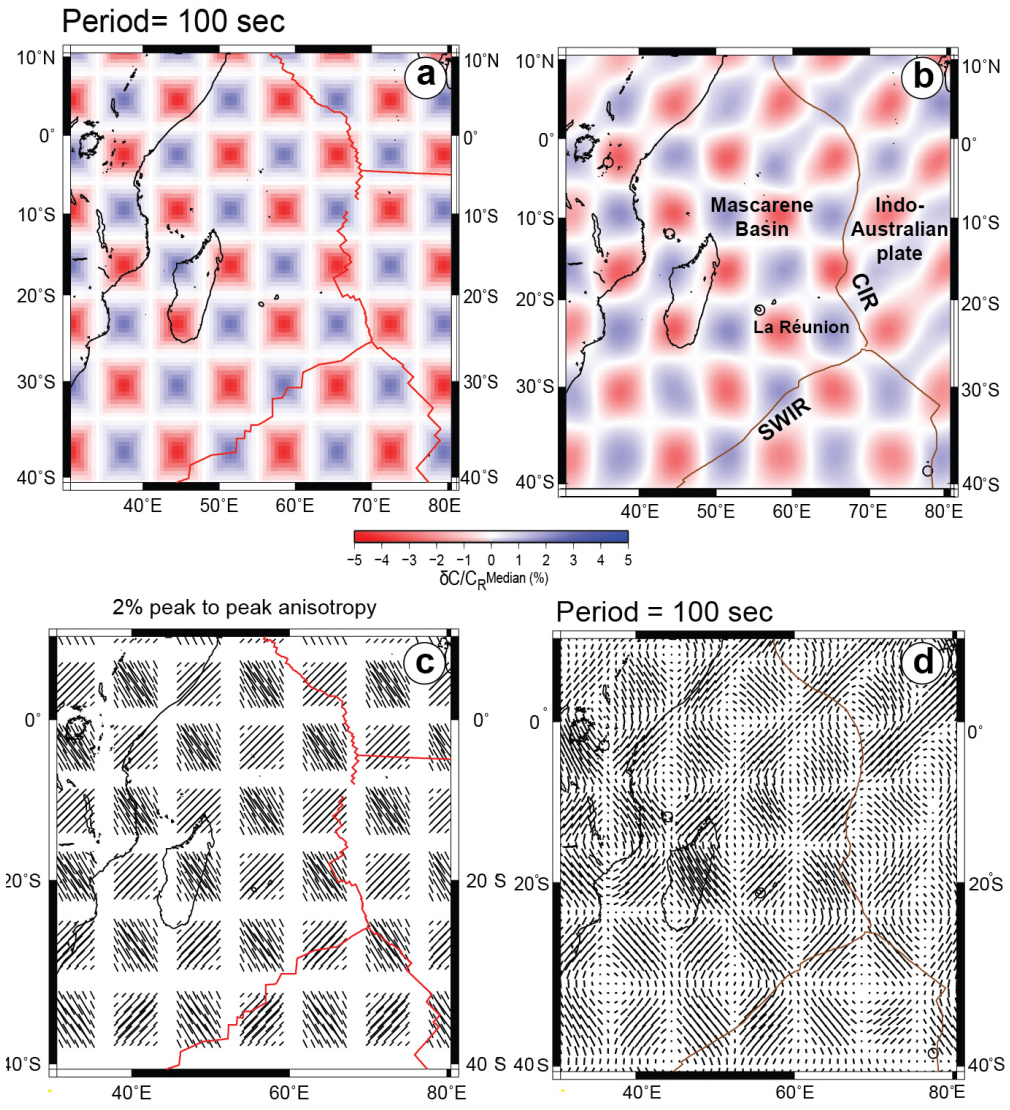

Figure S2

Figure S2: Synthetic tomography resolution test performed at 100s period. Left panels, we show the input velocity (a) and anisotropy structures (c). On the right panels, we show their respective recovery (b and d) from our actual ray coverage (Fig. S1). The slow and fast velocity structure, together with the azimuthal anisotropy pattern, are well recovered, particularly around Réunion, the Central Indian Ridge, and over the whole Mascarene Basin Asthenospheric Reservoir area (Fig. S1).

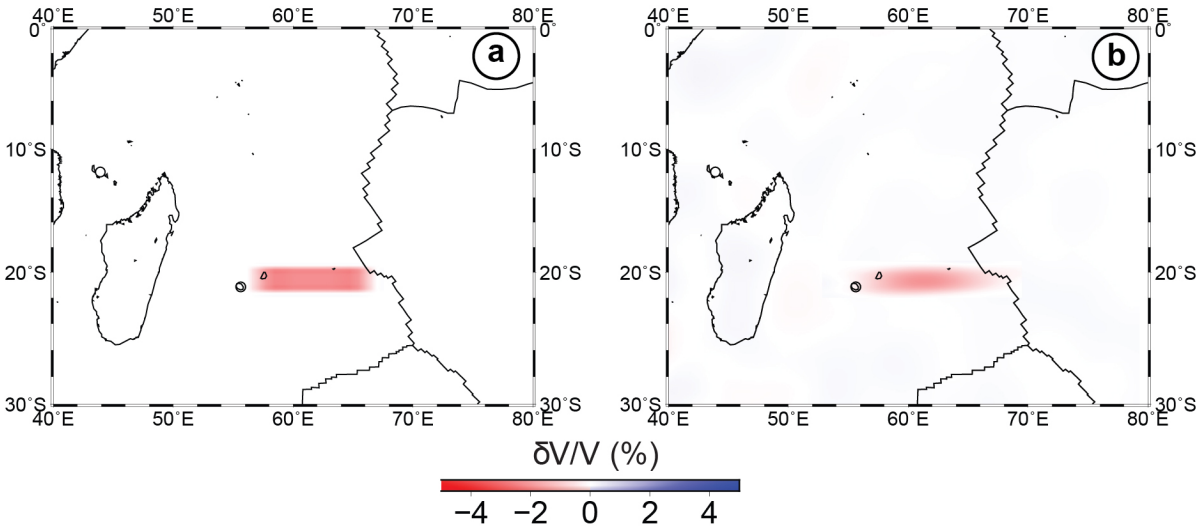

Figure S3

Figure S3: Synthetic tomography resolution test below the Rodrigues corridor. (a) Input is a slow velocity structure (*dVs/Vs* = -3%), sized 200km x 1000km, resembling the channel of slow asthenosphere present in the actual tomography model. (b) Resolution test output recovers the input well, with some smearing in east-west direction.

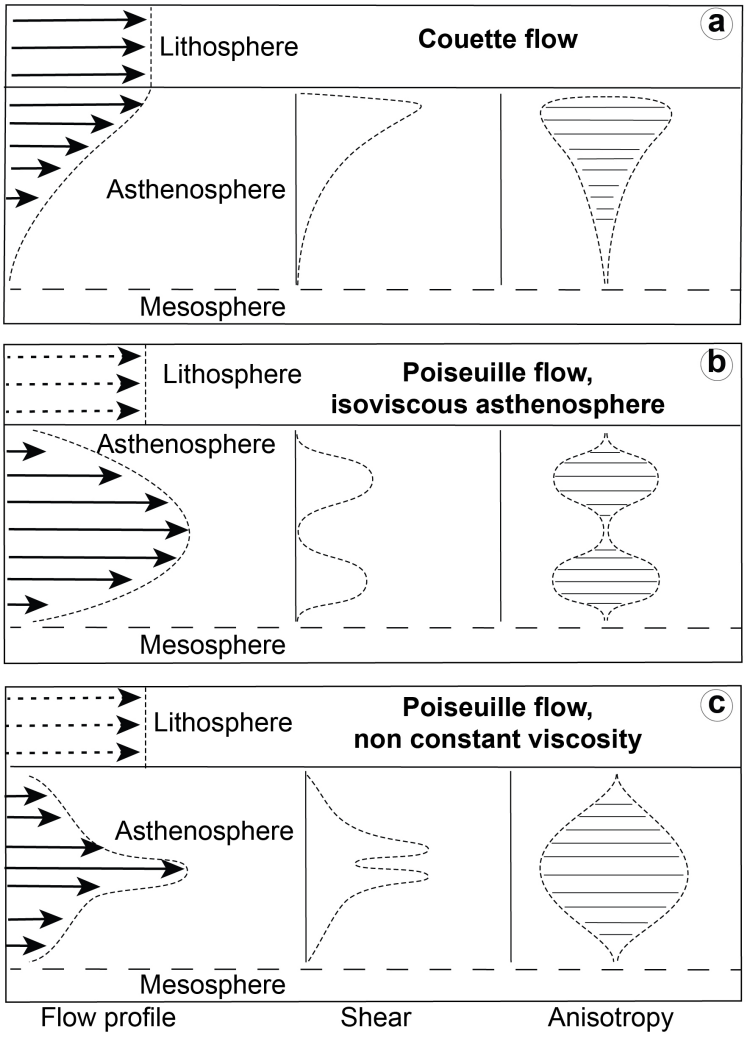

Figure S4

Figure S4: Development of anisotropy in the asthenosphere as a consequence of planar horizontal flow. In all panels, depth is plotted on the y-axis, showing a lithospheric layer above an asthenospheric layer ending at the asthenosphere-mesosphere boundary. Left panels: arrows show horizontal flow velocities as a function of depth. Middle panels: magnitude of shear strain as a function of depth. Right panels: magnitude of azimuthal anisotropy as a function of depth. The seismically fast direction is horizontal, the seismically slow direction is into and out of the figure plane.

(a) Couette flow: asthenosphere is passively dragged by the overlying lithosphere, which moves from left to right. Resulting strain and anisotropy are proportional to the vertical derivative of flow velocity, and peak just below the LAB. (b) Planar Poiseuille flow in an iso-viscous asthenosphere: a horizontal pressure gradient (from left to right) actively drives

horizontal flow in the asthenosphere. Lithosphere and asthenosphere are decoupled, i.e., lithospheric motion exerts no influence on flow in the asthenosphere. The asthenosphere is also decoupled from the underlying mesosphere. Strain and anisotropy have two well-separated lobes. (c) Poiseuille-like flow in a non-linear, mantle-like rheology: like case b), except that viscosity decreases towards the middle of the asthenosphere. This concentrates not only flow in the middle of the layer, but also its derivative, and therefore strain and anisotropy.

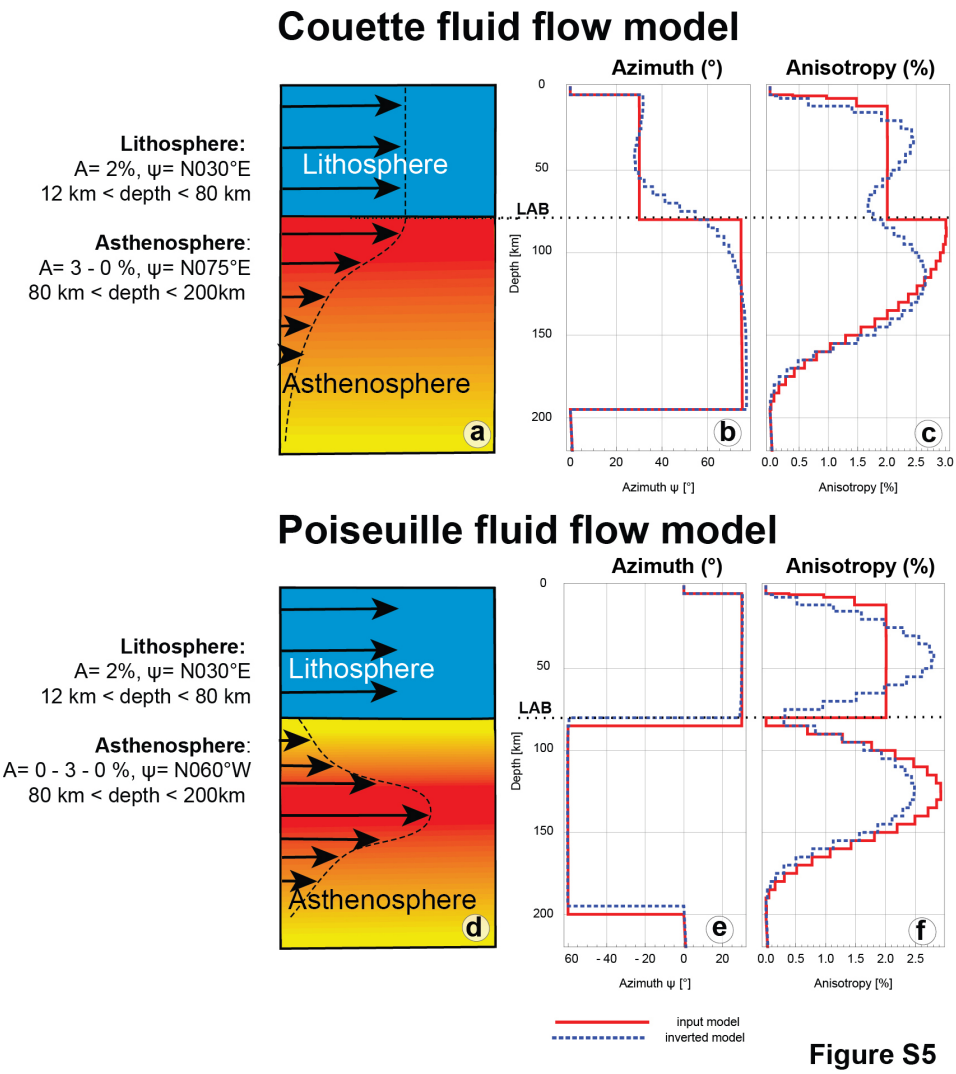

Figure S5

Figure S5: Tomographic resolution tests for the vertical distribution of anisotropy for the scenarios of planar Couette flow (top), and of planar Poiseuille flow in an asthenosphere that is weakest in the middle of the layer (bottom). The structure of fluid flow in each case is illustrated by panels (a) and (d). Lithosphere is shown in blue; in the asthenosphere, red regions support the highest shear and yellow regions are shearing less. Panels (b) and (e) show the seismically fast direction of azimuthal anisotropy as a function of depth: test inputs in red, recovered results in blue. Panels (c) and (f) show the magnitude of azimuthal anisotropy as a function of depth: inputs in red, recovered results in blue.

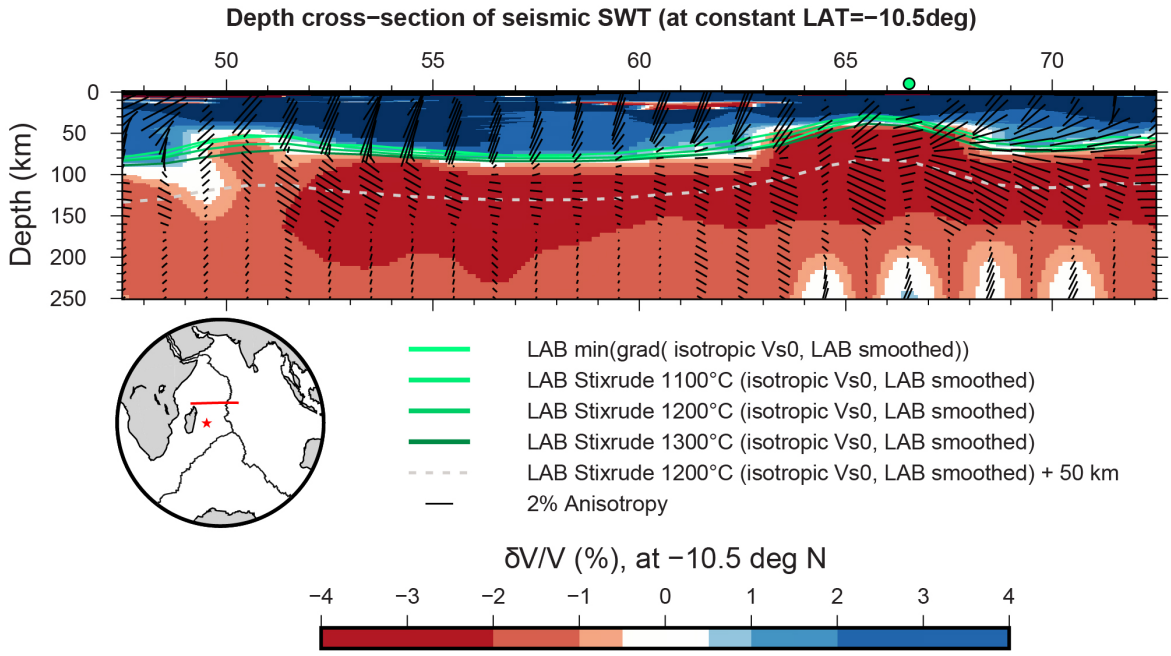

Figure S6

Figure S6: Estimating LAB depth. East-west cross section at 10.5°S through the Rayleigh wave tomography model of Mazzullo et al. (2017)[1], plotting styles as in main Fig. 4. Four lines in different shades of green represent different estimates of the lithosphere-asthenosphere boundary. Lightest green line traces the location of the steepest vertical gradient in isotropic *dVs/Vs* (Method 1). Three other green lines are LAB depths based on estimating the locations of the 1100°C, 1200°C and 1300°C isotherms[2] (Method 2). White dashed line runs 50 km below the estimated 1200°C isotherm[2], a rough estimate for the middle of the asthenospheric layer, which is used to plot azimuthal anisotropy on Fig. 3b.

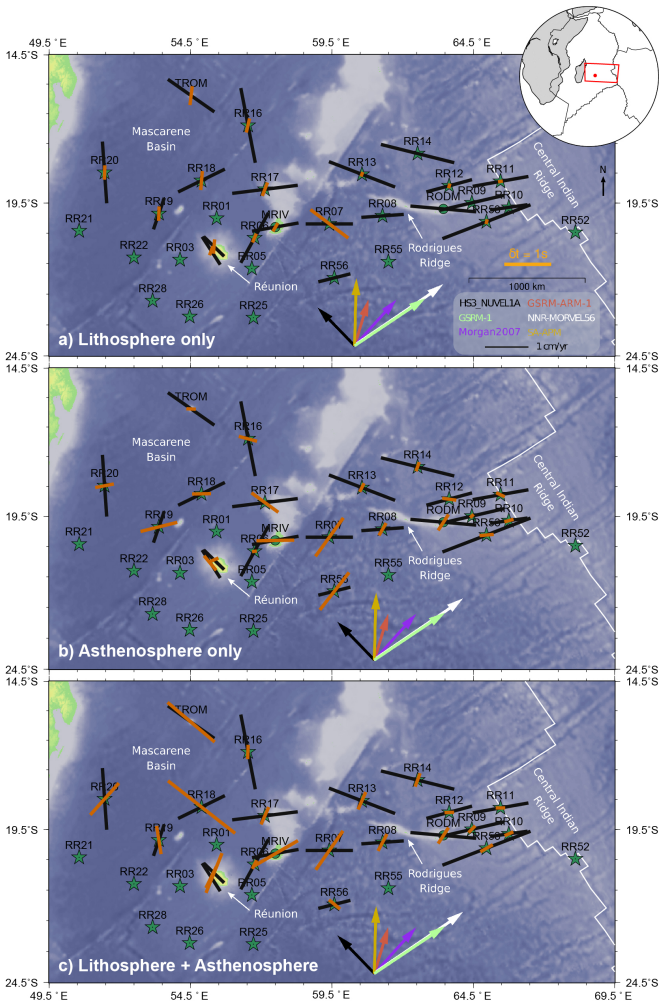

Figure S7

Figure S7: Observed versus tomography-predicted SKS splitting. Black bars are station-averages of measured SKS splitting parameters[3] in the area around the Réunion hotspot (red dot on inset map), Rodrigues corridor and Central Indian Ridge; orange bars are SKS splitting parameters forward-predicted through our Rayleigh-wave tomography model. SKS predictions were calculated for (a) only the lithosphere (25 km depth to LAB); (b) only the asthenosphere (LAB to 300 km depth); and (c) for the whole lithosphere + asthenosphere system (25 to 300 km depth). Coloured arrows indicate African (Somali) plate motion according to models HS3_NUVEL1A[4], GSRM-1[5], Morgan2007[6], GSRM-ARM-1[7], NNR-MORVEL56[8], and SA-APM[9]. First-order features are a general under-prediction of delay time magnitudes; good overall agreement between observed and predicted fast directions in the asthenosphere; and for the Rodrigues corridor, much larger delay times predicted for the asthenosphere than for the lithosphere, supporting the interpretation of anisotropy reflecting flow beneath the corridor.

References

1. Mazzullo A.*, et al.* Anisotropic Tomography around La Réunion Island from Rayleigh Waves. *J. Geophys. Res.*, **122**, 1-17 (2017).
2. Stixrude L. & Lithgow-Bertelloni C. Mineralogy and elasticity of the oceanic upper mantle: Origin of the low-velocity zone. *J. Geophys. Res.*, **110**, B03204 (2005).
3. Scholz J.-R.*, et al.* SKS splitting in the Western Indian Ocean from land and seafloor seismometers: Plume, Plate and Ridge signatures. *Earth Planet. Sci. Lett.*, **498**, 169-184 (2018).
4. Gripp A.E. & Gordon R.B. Young tracks of hotspots and current plate velocities. *Geophys. J. Int.*, **150**, 321-361 (2002).
5. Kreemer C., Holt W.E. & Haines A.J. An integrated global model of present-day plate motions and plate boundary deformation. *Geophys. J. Int.*, **154**, 8-34 (2003).
6. Morgan W.J. & Morgan J.P. Plate velocities in the hotspot reference frame. In: Foulger GR, Jurdy DM (eds). *Plates, plumes, and planetary processes*, vol. 430. Geological Society of America Special Paper, pp 65-78 (2007).
7. Kreemer C. Absolute plate motions constrained by shear wave splitting orientations with implications for hot spot motions and mantle flow. *J. Geophys. Res.*, **114**, B10405 (2009).
8. Argus D.F., Gordon R.G. & DeMets C. Geologically current motion of 56 plates relative to the no-net-rotation reference frame. *Geochem. Geophys. Geosyst*, **12**, Q11001 (2011).
9. Becker T.W., Schaeffer A.J., Lebedev S. & Conrad C.P. Toward a Generalized Plate Motion Reference Frame. *Geophys. Res. Lett.*, **42**, 3188-3196 (2015).
10. Seton M.*, et al.* Global continental and ocean basin reconstructions since 200Ma. *Earth-Science Reviews*, **113**, 212-270 (2012).
11. Wolfe C.J. & Solomon S.C. Shear wave splitting and implication for mantle flow beneath the MELT region of the East Pacific Rise. *Science*, **280**, 1230-1232 (1998).
12. Stotz I.L., Iaffaldano G. & Davies D.R. Pressure-Driven Poiseuille Flow: A Major Component of the Torque-Balance Governing Pacific Plate Motion. *Geophys. Res. Lett.*, **45**, 117-125 (2018).
13. Debayle E. & Ricard Y. Seismic observations of large-scale deformation at the bottom of fast-moving plates. *Earth Planet. Sci. Lett.*, **376**, 165-177 (2013).
14. Takeo A.*, et al.* Seismic azimuthal anisotropy in the oceanic lithosphere and asthenosphere from broadband surface wave analysis of OBS array records at 60 Ma seafloor. *J. Geophys. Res.*, **121**, 1927–1947 (2016).
15. Natarov S.I. & Conrad C.P. The role of Poiseuille flow in creating depth-variation of asthenospheric shear. *Geophys. J. Int.*, **190**, 1297-1310 (2012).